Post-Depositional Fluid Flow in Jurassic Sandstones of the Uncompahgre Uplift: Insights From Magnetic Fabrics

John I. Ejembi[1]*, Eric C. Ferré[2], Sara Satolli[3] and Sarah A. Friedman[4]

[1]Department of Geology, Southern Illinois University, Carbondale, IL, United States, [2]School of Geosciences, University of Louisiana at Lafayette, Lafayette, LA, United States, [3]Department of Engineering and Geology, University "G. d'Annunzio", Chieti-Pescara, Italy, [4]Department of Biological and Physical Sciences, Montana State University Billings, Billings, MT, United States

The anisotropy of magnetic susceptibility (AMS) in sedimentary rocks results from depositional, diagenetic, syn- and post-sedimentary processes that affect magnetic grains. Some studies have also shown the potential role played by post-depositional fluid flow in detrital and carbonate formations. Here we present a new case study of Middle-Upper Jurassic sandstones where secondary iron oxides, precipitated from fluids that migrated through pores, give rise to the AMS. These sandstones are well exposed in the Uncompahgre Uplift region of the Central Colorado Trough, Colorado. The magnetic foliation of these undeformed, subhorizontal strata consistently strike NE-SW over a large distance with an average 45° dip to the SE. This steep AMS fabric is oblique with respect to the regional subhorizontal bedding and therefore does not reflect the primary sedimentary fabric. Also, outcrop-scale and microscopic observations show a lack of post-depositional plastic (undulose extinction) or pressure-solution (stylolites) deformation microstructures in these sandstones, hence precluding a tectonic origin. The combination of magnetic hysteresis, isothermal remanent magnetization, and thermal demagnetization of the natural remanent magnetization indicate that these rocks carry a chemical remanent magnetization born primarily by hematite and goethite. High-field magnetic hysteresis and electron microscopy indicate that detrital magnetite and authigenic hematite are the main contributors to the AMS. These results show that post-depositional iron remobilization through these porous sandstones took place due to the action of percolating fluids which may have started as early as Late Cretaceous along with the Uncompahgre Uplift. The AMS fabric of porous sandstones does not systematically represent depositional or deformation processes, and caution is urged in the interpretation of magnetic fabrics in these types of reservoir rock. Conversely, understanding these fabrics may advance our knowledge of fluid flow in porous sandstones and may have applications in hydrocarbon exploration.

Keywords: anisotropy of magnetic susceptibility, fluid flow, Jurassic, Uncompahgre uplift, central Colorado, sediment

FIGURE 1 | Geologe map of the study area in western Colorado (after Tweto and Schoenfeld, 1979) and a northwest to southeast trending geologic cross-section of the study sites. The depth profile across section according to USGS DEM maps of area.
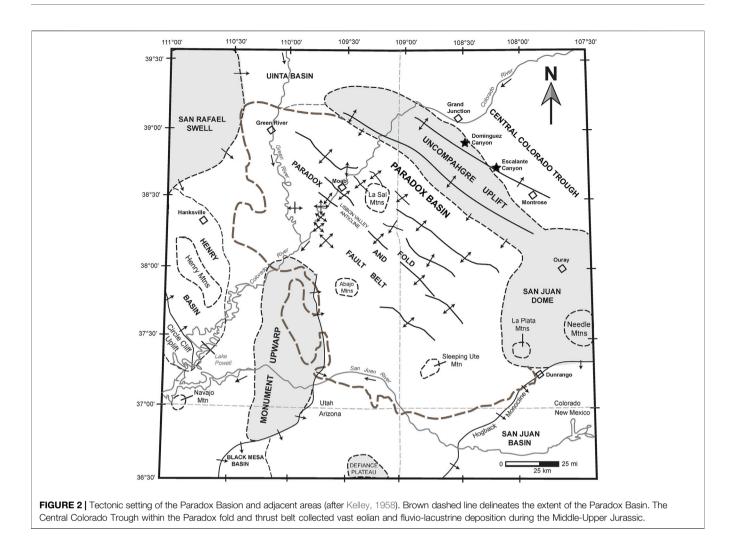
INTRODUCTION

Fluid-flow through permeable sandstones is a key process in multiple economically important geological processes such as, hydrocarbon migration (e.g., Oliver, 1986; Hunt, 1990; Ungerer et al., 1990), diagenetic alteration through fluid-rock interaction (Chan et al., 2000; Beitler et al., 2005; Potter and Chan, 2011; Potter-McIntyre et al., 2014), groundwater contamination of aquifers (e.g., Massei et al., 2002), or fluid-driven precipitation of ore minerals (e.g., Wilkinson, 2001). Common approaches to characterize regional fluid flow through rocks include fluid geochemistry (Musgrove and Banner, 1993) and hydrodynamic flow models (Wing and Ferry, 2007). For example, Musgrove and Banner (1993) used elemental and stable isotopic signatures in groundwater samples from a Cambro-Ordovician and Mississippian aquifer that were collected from different wells to evaluate the origin and mixing of meteoric and saline fluids in the United States Midcontinent. This approach relies on direct sampling of fluids for geochemical analysis and modeling whereas the hydrodynamic model approach requires multiple topographic relationships to be maintained for an accurate prediction of fluid-flow directions. These approaches, although generally successful, have limited application in ancient geologic systems particularly when fluid-flow is no longer active or when the original paleotopography has been modified either through erosion, alteration or tectonic activity.

In this study, we investigate the magnetic mineralogy, the origin and significance of the anisotropy of magnetic susceptibility (AMS), the NRM, and their implications regarding regional-scale fluid migration. The Jurassic sandstones of this study originate from two sites, located 12 km apart, along the southwest margin of the Central Colorado Trough, on the Eastern flank of the Uncompahgre Uplift: Escalante Canyon—EC and Dominguez Canyon, also known as Bridgeport—BP (**Figures 1**, **2**). The study area in the western Colorado Plateau consists primarily of Mesozoic sedimentary rocks underlain by deeply faulted Proterozoic crystalline basement blocks (**Figure 1**; e.g., Marshak et al., 2000). The Cenozoic and some Late Mesozoic sedimentary formations in this region have been eroded through successive uplifts (**Figures 1**, **2**; Pederson et al., 2002).

AMS has been an effective tool for tracking paleofluid flow in sedimentary rocks, magma flow in igneous provinces, and hydrothermal fluids caused by mantle upwelling (e.g., Schieber and Ellwood, 1993; Ferré et al., 2002; Sizaret et al., 2006; Essalhi et al., 2009). This method is sensitive to the petrofabric and crystallographic orientations of magnetic mineral grains (Tarling and Hrouda, 1993). The AMS of sediments has been successfully used to characterize syn- and post-depositional processes in sedimentary systems since its introduction by Ising (1942). Examples have been shown for geometry of pore spaces in siliciclastic rocks (Robion et al., 2014; Parés et al., 2016), flow mechanisms and nature of sediment deposition (Dall'Olio et al., 2013), and microscopic strain and deformational structures (e.g., Aubourg et al., 2004; Aubourg et al., 2010; Robion et al., 2007; Burmeister et al., 2009).
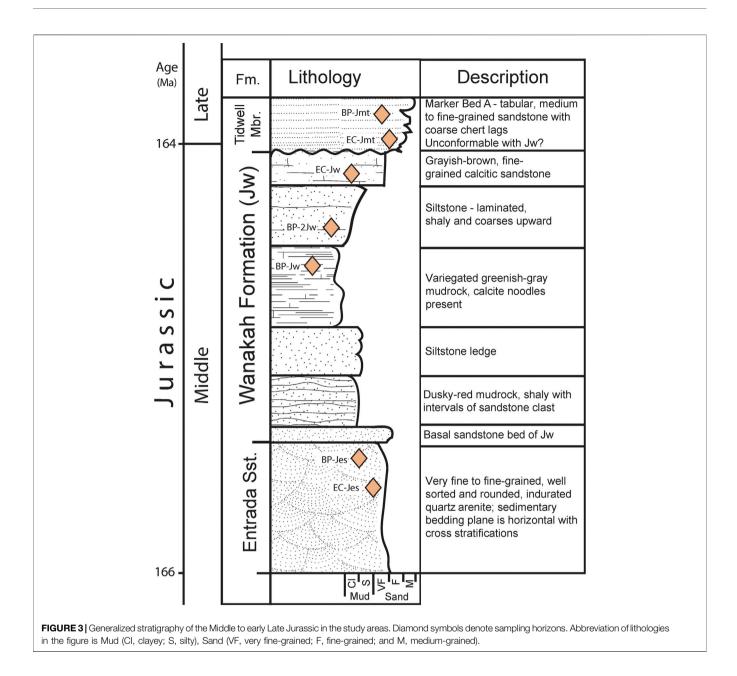
FIGURE 2 | Tectonic setting of the Paradox Basion and adjacent areas (after Kelley, 1958). Brown dashed line delineates the extent of the Paradox Basin. The Central Colorado Trough within the Paradox fold and thrust belt collected vast eolian and fluvio-lacustrine deposition during the Middle-Upper Jurassic.

The maroon, red, pink and in some cases, tan to grayish colors of the Middle-Late Jurassic sandstones of the Entrada Sandstone, Wanakah Formation, and Tidwell Member of the Morrison Formation in the Paradox Basin and adjacent areas are classic examples of secondary coloration acquired through fluid flow in permeable rocks (Parry et al., 2004; Beitler et al., 2005). The extent to which a primary and depositional fabric is preserved in these rocks, as opposed to a pervasive chemical overprint, constitutes the focus of this study. The magnetic mineralogy itself, along with the magnetic grain morphology, provide useful information on the syn- or post-depositional origin of the AMS. While radiometrically dating the development of the AMS is generally difficult, the paleomagnetic data acquired in our investigations could shed light on the type of AMS in these sandstones. The hypothesis we test using paleomagnetic data, combined with a well-established regional Jurassic-Cretaceous magnetostratigraphy, is that the AMS was acquired during or shortly after deposition, and therefore reflects primarily the sediment transport direction. The alternative hypothesis is that the AMS records a late stage precipitation event related to

the downcutting of the Colorado and Gunnison Rivers (Hunt, 1969; Cook et al., 2009).

TECTONIC SETTING

The study area is situated on the northeastern margin along the Northeast flank of the Uncompahgre Plateau, west of the Central Colorado Trough (**Figure 2**). To the Southwest of the study area, the Paradox Basin formation began with crustal loading and downward lithospheric flexure during the contractional Pennsylvanian–Permian orogeny that formed the Ancestral Rocky Mountains (**Figure 2**; Kluth and Coney, 1981; Barbeau, 2003). Basin subsidence continued from the Triassic through Cretaceous. The Paradox Basin and other adjacent basins consist of Paleozoic through Cenozoic strata that unconformably overlie Proterozoic basement rocks that include granitic, high-grade metamorphic gneiss and schist (Tweto and Schoenfeld, 1979; **Figure 2**). Cretaceous rocks exposed on the Colorado Plateau have mostly been eroded away due to subsequent uplift and downcutting of major

FIGURE 3 | Generalized stratigraphy of the Middle to early Late Jurassic in the study areas. Diamond symbols denote sampling horizons. Abbreviation of lithologies in the figure is Mud (Cl, clayey; S, silty), Sand (VF, very fine-grained; F, fine-grained; and M, medium-grained).

fluvial drainages (**Figure 1**). The Paradox Basin shows a prominent fold-and-fault belt defined by NW-SE striking faults, anticlines, and synclines (**Figure 2**). Some of these structures are related to salt walls and grabens caused by diapirism of the Paradox Formation (Nuccio and Condon, 1996).

The tectonic layer-parallel shortening (LPS) axis in the Paradox Basin is oriented NE-SW, parallel to the maximum principal stress (**Figure 2**). Kluth and Coney (1981) interpreted the orientation of this axis and the Ancestral Rocky Mountains as part of a complex intraplate response in the western United States due to the Ouachita-Marathon orogeny, a collision of the North American craton with South America and Africa during the Pennsylvanian. These authors also

suggested that the suturing at the southern margin of the North American craton combined with northward directed thrusting from the Marathon region led to a progressive migration of stresses onto the continental interior. Other studies have suggested that 1) the origin of the Paradox Basin structures might be related to compressive stresses from either the Ancestral Rockies or Laramide orogenic events (Marshak et al., 2000) or 2) these structures predates these events but were reactivated along pre-existing faults in the basement (Davis, 1978; Baars and Stevenson, 1981).

The Uncompahgre Uplift was originally interpreted as a Pennsylvanian structure associated with the formation of the Ancestral Rocky Mountains (e.g., Kluth and Coney, 1981). However, recent thermochronological constraints document a

far more recent uplift history beginning in the Late Cretaceous (Laramide orogeny) and continuing with deep incision up to the Miocene-Pliocene (Rønnevik et al., 2017).
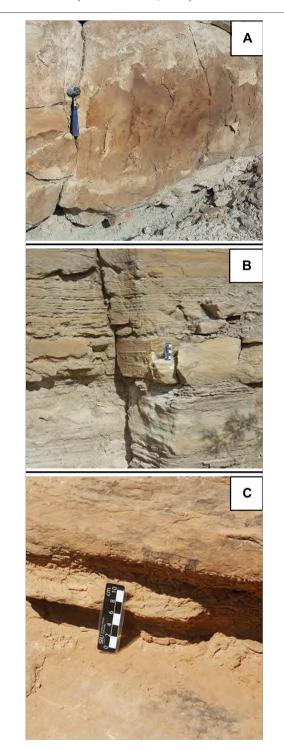

FIGURE 4 | Field photographs showing sedimentary bedding and sandstone lithologies of **(A)**. Marker Bed A - the basal sandstone of the Tidwell Mbr. of Morrison Fm. Marker Bed A is the sandstone bed that separates the Middle and Late Jurassic rocks. **(B)** Wanakah Fm. and **(C)** Entrada Sandstone. Hammer and scale bars are for scale.
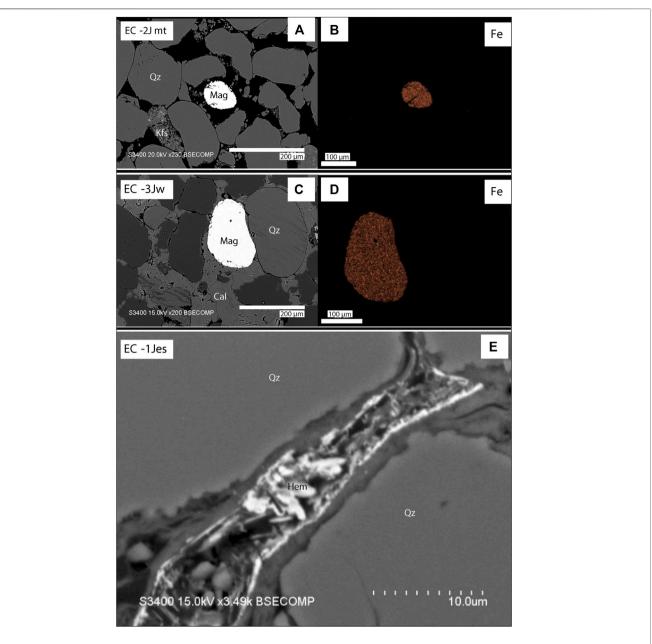
ANALYTICAL METHODS
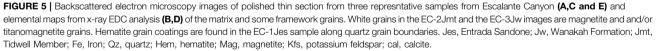
Sampling and Petrography

From oldest to youngest, we collected hand samples (with an average dimension of $15 \times 12 \times 8$ cm) from the Entrada Sandstone, the Wanakah Formation, and the Tidwell Member of the Morrison Formation (**Figure 3**). Hand samples were georeferenced using hand-held Global Positioning System units (GPS). The geographic orientation of the samples was determined using a magnetic compass, after correction of the magnetic declination (11˚E). Hand samples were extracted using a rock hammer to obtain fresh surfaces and to avoid supergene alteration overprints. The sandstones exhibit light brown to pale tan colors in the Tidwell Member of the Morrison Formation (**Figures 4A**), brown, pink or tan colors in the Wanakah Formation (**Figures 4B**) and relatively bright red to orange colors in the Entrada Sandstone (**Figures 4C**). These colors attest to the presence of iron oxides and hydroxides cement in the bulk sample. Polished petrographic thin-sections were prepared for selected, representative specimens to assess the mineralogy, morphology and grain size of the constituent mineral phases. The thin-sections were examined using a Hitachi S-3400N scanning electron microscope (SEM) in backscatter (BSE) mode at Montana State University Billings. Additional analyses with an energy dispersive spectroscopy (EDS) Ametek EDAX system provided semi-quantitative spot chemical analyses. Before imaging, thin-sections were coated with a 45 Å-thick layer of gold/palladium to prevent charging. The operation conditions of 15–20 kV accelerating voltage and a working distance of 10.0 μm yielded the best results.

Anisotropy of Magnetic Susceptibility Measurements

We cut several serial 2 cm-thick slabs from the hand samples to produce 2 cm sample cubes. The 2 cm AMS cubes were cut, side-by-side, from these slabs to yield about 15 cubic specimen per one hand sample. These oriented cubes were measured using the AGICO KLY-4S Kappabridge susceptibility meter at Southern Illinois University Carbondale. Measurements were performed at room temperature with an applied magnetic field of 300 A/m and frequency of 875 Hz. The AMS measurements were processed using the AGICO SUFAR program while the acquired data were plotted using the AGICO Anisoft 4.2 program. Directional data obtained from the projection of the three principal magnetic susceptibility axes on equal-area lower hemisphere stereonets, including their 95% confidence ellipses, were calculated using the Jelinek statistics (Jelínek, 1978; **Supplementary Material**).

The AMS is defined by a symmetric, second-rank tensor consisting of six independent elements represented by an ellipsoid with three mutually perpendicular axes. The three axes represent the three principal magnetic susceptibilities namely: K_1 (maximum), K_2 (intermediate), and K_3 (minimum). The AMS parameters used in this study include the mean magnetic susceptibility $K_m = \left(\frac{K_1 + K_2 + K_3}{3} \right)$, indicative

FIGURE 5 | Backscattered electron microscopy images of polished thin section from three represntative samples from Escalante Canyon **(A,C and E)** and elemental maps from x-ray EDC analysis **(B,D)** of the matrix and some framework grains. White grains in the EC-2Jmt and the EC-3Jw images are magnetite and and/or titanomagnetite grains. Hematite grain coatings are found in the EC-1Jes sample along quartz grain boundaries. Jes, Entrada Sandone; Jw, Wanakah Formation; Jmt, Tidwell Member; Fe, Iron; Qz, quartz; Hem, hematite; Mag, magnetite; Kfs, potassium feldspar; cal, calcite.

of the concentration of magnetic minerals present in the hand sample; the degree of magnetic anisotropy P' where $a_1 = ln\left(\frac{K_1}{K_m}\right)$, $a_2 = ln\left(\frac{K_2}{K_m}\right)$, and $a_3 = ln\left(\frac{K_3}{K_m}\right)$, which describes the strength of the magnetic fabric, and in general is a proxy for the type of magnetic fabric in the rocks; and the shape factor $T = 2\left((\ln K_2 - \ln K_3)/(\ln K_1 - \ln K_3)\right) - 1$, which represents the shape of the ellipsoid of the magnetic fabric (oblate or prolate), with T ranging from −1 to +1, prolate (with T ≤ 0) and oblate (with T ≥ 0).

Magnetic Hysteresis and Isothermal Remanent Magnetization Measurements

We performed both magnetic hysteresis experiments and Isothermal Remanent Magnetization (IRM) experiments at room temperature, on rock fragments to identify the nature of the AMS carriers. Magnetic hysteresis was measured on 11 specimens using the MicroMag 3900-04 vibrating sample magnetometer (VSM; Princeton Measurements Corporation) at Southern Illinois University Carbondale. IRM experiments were performed on two representative specimens with

TABLE 1 | Magnetic hysteresis properties of Middle-Late Jurassic sandstones from the Paradox Basin, western Colorado.

	Sample	Ms µAm²	Mr µAm²	Hc mT	Hcr mT	Mr/ Ms	Hcr/ Hc	HF Slope µAm²/T	Hysteresis Loop
Dominguez	BP-2Jmt	1.33	0.32	20.63	66.24	0.24	3.21	+6.13	A
Canyon	BP-1Jmt	1.98	0.48	20.41	69.89	0.24	3.42	+11.04	A
	BP-2Jw	1.48	0.31	19.74	90.46	0.21	4.58	+17.60	A
	BP-1Jw	1.67	0.38	22.35	141.60	0.23	6.34	0.00	A
	BP-2Jes	1.79	0.54	40.98	188.30	0.30	4.59	+1.21	B
	BP-1Jes	2.25	0.81	54.70	202.10	0.36	3.69	+1.02	B
Escalante Canyon	EC-2Jmt	1.28	0.24	16.98	63.23	0.19	3.72	+14.21	A
	EC-1Jmt	1.51	0.27	12.55	49.46	0.18	3.94	+19.39	A
	EC-1Jw	1.13	0.14	10.80	41.03	0.12	3.80	+6.77	A
	EC-2Jes	6.94	2.18	39.82	158.80	0.31	3.99	+10.66	B
	EC-1Jes	4.24	1.48	42.35	175.70	0.35	4.15	−7.37	B

contrasting colors (one specimen from each locality). A field strength of up to 1.5 T was applied to saturate the specimens magnetically. For comparison, the induced magnetization in both specimens was normalized after correcting for high-field slope, in this case, 70% of the maximum applied field.

Paleomagnetic Measurements

Due to the assumed presence of hematite in the hand samples, we chose thermal demagnetization of the NRM to constrain the different magnetic phases present in each specimen. Thermal demagnetization of the NRM was performed at the CIMaN-ALP laboratory of paleomagnetism (Peveragno, Italy) using a Superconducting Rock Magnetometer 2G Enterprise 755 hosted in a shielded room. Forty-eight representative AMS cubes (16 per formation) were selected for thermal demagnetization of the NRM. The specimens were subjected to a stepwise thermal demagnetization in 15 steps from room temperature to 600°C, with additional four steps up to 700°C for specimens showing higher unblocking temperatures.
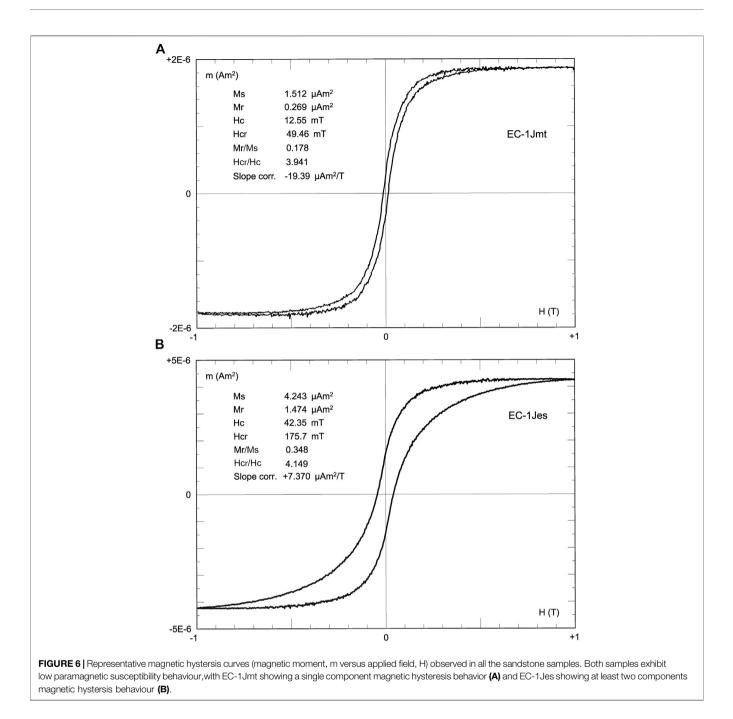
RESULTS

Petrographic Analysis

Previous work reports on the petrographic characteristics of the Entrada Sandstone, Wanakah Formation and Tidwell Member of the Morrison Formation (Ejembi et al., in review). Based on Folk (1980) sandstone classification, the Entrada Sandstone consists dominantly of sublitharenites, while the Wanakah Formation and Tidwell Member range from feldspathic litharenite to litharenite. The Entrada Sandstone in the two localities is predominantly pinkish to reddish brown, cross-bedded, and is composed of fine to very fine-grained, sub-rounded to rounded framework grains. The Wanakah Formation consists of distinct, thin beds (<0.15 m) of fine-grained sandstone with interbedded mudrocks that have a characteristic red and green color. The Tidwell Member consists of a regionally extensive, dark gray to tan, marker sandstone bed with overlying beds that are tabular, coarse-

grained, and are interbedded with mudrocks. These sandstone beds vary in thicknesses (0.7–1.5 m), with a maximum measured thickness of ~1.5 m at Escalante Canyon.

The quartz and feldspar grains in these units are strikingly free of any transgranular or intergranular deformation fractures and inherited or cognate plastic deformation microstructures such as undulose extinction. Both optical microscopy and scanning electron microscopy reveal very pristine detrital grains assembled in undeformed, fabric-less assemblages. Cross-bedding structures, when present, result from grain size variation. **Figure 5**, for example, shows representative SEM-BSE images of polished thin sections along with corresponding maps of major elements from the sandstone specimens using x-ray energy-dispersive systems (EDS) analysis. The maps of iron distribution in the matrix reveal no specific coating along grain margins. The EDS chemical analyses help identify quartz, alkali feldspar, calcium carbonates, and iron oxides/hydroxides. However, magnetite and titanomagnetite detrital grains were observed in some of the specimen (based on the Fe, O and Ti elemental maps, e.g., EC-2Jmt and EC-3Jw (**Figure 5**). This lack of ferromagnetic grains is not unusual in terrestrial sandstones where these minerals are quickly degraded and precipitated as early hematite grain coatings (e.g., Chan et al., 2007).

Magnetic Hysteresis Properties and Isothermal Remanent Magnetization Behavior

The hysteresis behaviors show negligible contributions of diamagnetic minerals, minor contributions of paramagnetic minerals, and the dominance of ferromagnetic phases (**Table 1** and **Figure 6**). The magnetic hysteresis parameters, saturation magnetization (M_s), saturation remanent magnetization (M_r), and magnetic coercivity (H_c) are calculated after correction of the high field slope, which arises primarily from the sum of diamagnetic (quartz and carbonates) and paramagnetic (clay and other detrital grains) and antiferromagnetic contributions. The coercivity of remanence (H_{cr}) was determined through back-
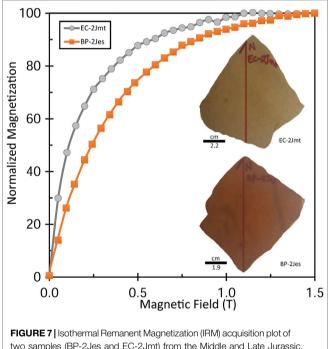
FIGURE 6 | Representative magnetic hystersis curves (magnetic moment, m versus applied field, H) observed in all the sandstone samples. Both samples exhibit low paramagnetic susceptibility behaviour, with EC-1Jmt showing a single component magnetic hysteresis behavior **(A)** and EC-1Jes showing at least two components magnetic hystersis behaviour **(B)**.

field experiments. Two fundamental behaviors are observed: a single phase with a low to moderate remanent coercivity phase (e.g., EC-1Jmt, $H_{cr} \approx 49.5$ mT; **Figures 6A**); and a two-phase mixture with high- and moderate-coercivity phases resulting in a wasp-waisted shaped hysteresis loop (e.g., EC-1Jes, $H_{cr} \approx 176$ mT; **Figures 6B**). Most specimens reach magnetic saturation at fields above 0.6 T. A few specimens show a negative high-field slope (e.g., EC-1Jes) indicative of a very small diamagnetic contribution. As the contribution of the high-coercivity phase is highly variable, the M_r/M_s and H_{cr}/H_c ratios result from a

mixture of several single-phase properties and therefore cannot be used as indicators of magnetic granulometry. The relatively low values of the high field slope (**Table 2**) indicate that paramagnetic phases cannot account for the observed AMS.

Two types of IRM acquisition behavior for specimens with contrasting lithofacies (i.e., color, texture, and porosity) are shown in **Figure 7**. The IRM plots show distinct approaches to magnetic saturation up to 1.5 T. These differences correlate with the color of the specimen: red sandstones are more magnetically coercive than tan sandstones.

TABLE 2 | Average scalar and tensorial AMS data of Middle-Upper Jurassic sandstones from the Paradox Basin, western United States.

| Field Location / | No of AMS data | Km × 10-6 [SI] | | P' | | | T | | |
		Scalar mean	Stand. dev	Tensorial mean	Scalar mean	Stand. dev	Tensorial mean	Scalar mean	Stand. dev
Dominguez Canyon, CO									
BP-2Jmt	25	14.80	1.52	1.077	1.088	0.028	0.460	0.346	0.381
BP-1Jmt	18	19.50	1.69	1.027	1.029	0.005	0.306	0.241	0.283
BP-2Jw	15	20.20	1.95	1.050	1.052	0.015	0.570	0.322	0.292
BP-1Jw	18	26.20	1.42	1.020	1.020	0.003	0.110	0.060	0.266
BP-2Jes	16	13.29	1.92	1.072	1.082	0.014	0.042	0.045	0.342
BP-1Jes	20	9.70	1.50	1.154	1.181	0.044	0.215	0.081	0.272
Escalante Canyon, CO									
EC-2Jmt	20	23.60	1.84	1.017	1.021	0.007	0.408	0.281	0.332
EC-1Jmt	20	26.91	1.78	1.053	1.063	0.011	0.438	0.189	0.213
EC-1Jw	6	8.14	0.86	1.108	1.123	0.023	0.154	0.168	0.431
EC-2Jes	12	25.10	3.89	1.025	1.036	0.011	0.086	0.195	0.318
EC-1Jes	13	30.50	2.01	1.020	1.029	0.006	0.297	0.203	0.451

Km, magnetic susceptibility; P', degree of anisotropy; T, shape factor; K1, K2, and K3 are the maximum, intermediate, and minimum magnetic susceptibility axes, respectively. The mean direction and confidence ellipses of the susceptibility axes are calculated using the Jelinek statistics in Anisoft 4.2 software.

FIGURE 7 | Isothermal Remanent Magnetization (IRM) acquisition plot of two samples (BP-2Jes and EC-2Jmt) from the Middle and Late Jurassic, respectively. The two samples are remarkably different lithologically. Insets are photographs of a freshly cut slab of both samples taken during the AMS sample preparation stage. The marker on the sample surface shows the in situ geographic orientation.
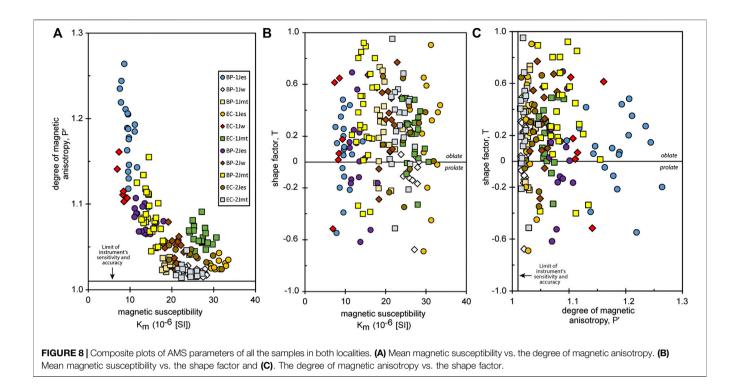
Anisotropy of Magnetic Susceptibility

The AMS scalar parameters (K_m, T, and P') are plotted in binary diagrams in **Figure 8** and provided in **Table 2**. The specimens display consistent magnetic properties. P' shows a negative correlation with K_m, both at the scale of the specimen and across specimens. K_m ranges from ~8.14 to 31.0 × 10^{-6} SI (**Figures 8A**). There is no correlation between the rock color and AMS parameters. P' ranges from 1.02 to 1.27, clearly

outside the range of values attributed to paramagnetic only assemblages, but most specimens have P' < 1.05 (**Figures 8B**). T varies substantially within each specimen but overall shows mainly oblate symmetry (**Figures 8C**). Although the degree of anisotropy in the specimens is strongly influenced by the weak magnetic susceptibility, it does not provide a reliable estimate of the strain at magnetic susceptibilities close to zero.

The stereonets of the three principal magnetic susceptibility axes (K_1, K_2, and K_3) obtained from the sandstone specimens from the two study sites are shown in **Figure 9**. The 95% confidence ellipses around averages per specimen are derived from the Jelinek statistics (Jelínek, 1978). The AMS directional parameters are rather consistent at the hand sample scale and between specimens. The specimens display a strong and consistent—but varying degree of steepness of the—magnetic foliation (planar fabric) defined by the K_1–K_2 plane (**Figure 9**), which dips to the SE. The double arrow shows the dip angle of the magnetic foliation. The magnetic lineation (K_1) is moderately well-defined and show discrete clusters. The AMS planar fabric of these rocks is clearly oblique with respect to the sub-horizontal bedding plane observed on the outcrop where each hand sample was collected from.

Thermal Demagnetization of the NRM

Stepwise thermal demagnetization of the NRM is shown for six out of forty-eight representative specimens in **Figure 10**. The NRM intensities range from 3.69×10^{-5} to 9.91×10^{-3} A/m, with an average of 1.86×10^{-3} A/m. Characteristic remanent magnetizations (ChRMs) were successfully isolated in 39 (over 48) specimens, both with normal (16 specimens) and reversed polarities (23 specimens). In most cases, the experiments show a stable single-component behavior, with a relatively straight ChRM toward the origin. Few specimens show evidence of a second directional components, isolated at lower temperatures (e.g., BP-1Jmt), including some with normal and reverse components. The ChRMs are scattered, and do not pass the

FIGURE 8 | Composite plots of AMS parameters of all the samples in both localities. **(A)** Mean magnetic susceptibility vs. the degree of magnetic anisotropy. **(B)** Mean magnetic susceptibility vs. the shape factor and **(C)**. The degree of magnetic anisotropy vs. the shape factor.

reversal test (McFadden and McElhinny, 1990). The weakly magnetized specimens (which were independent of the formation or lithology) that lack stable demagnetization behaviors could not be interpreted. In most specimens from the Tidwell Member and the Wanakah Formation, the main demagnetization occurs below 150°C while the remainder is generally removed below 300°C (e.g., **Figures 10A–D**). Most specimens from the Entrada Sandstone also display demagnetization below 150°C, but some retain part of their magnetization up to 500°C–680°C (e.g., **Figures 10F**). The stable demagnetization directions vary substantially in inclination (**Figure 10**) with an average ~55° for the <150°C stable component, while the variations in magnetic declination are also high.

DISCUSSION

Origin and Development of Anisotropy of Magnetic Susceptibility Fabrics in Sedimentary Rocks

Previous studies have shown that the origin of magnetic fabrics in sedimentary rocks is controlled by sedimentary vs. tectonic processes (e.g., Tarling and Hrouda, 1993; Li et al., 2014). The sedimentary origin of AMS lies in the depositional process by which particles settling in a slurry acquire a shape preferred orientation parallel to the depositional plane, which is close to horizontal in most cases. The compaction of sediments generally strengthens the planar component of the syn-depositional fabric because it results from the application of a vertical stress (gravity).

When bedding is horizontal, there is either no lineation of the maximum susceptibility, or a very weak lineation. Regardless of the magnetic carriers, the resulting AMS tends to be strongly planar and weakly linear, i.e., oblate fabrics (e.g., Schieber and Ellwood, 1993; Tarling and Hrouda, 1993; Saint-Bezar et al., 2002; Aubourg et al., 2004; Aubourg et al., 2010; Parés et al., 2007; Robion et al., 2007; Dall'Olio et al., 2013). Sedimentary magnetic fabrics in sedimentary rocks are characterized by a tight clustering of the K_3 axis along the bedding pole, with the K_1 and K_2 axes dispersed within the bedding plane (**Figures 11A**). In rare cases, eolian sedimentary rocks may acquire a linear fabric parallel to the wind direction (e.g., Lagroix and Banerjee, 2002). For materials deposited under a strong current, a linear fabric parallel to the current may be imparted, although such fabrics are typically reported in shales and rarely in sandstones (e.g., Ellwood and Howard, 1981; Schieber and Ellwood, 1993; Tarling and Hrouda, 1993), and the amplitude of the imbrication angle of deposited sediments is very small compared to the strongly oblique magnetic fabric observed in our specimens (**Figures 11B**).

Tectonic overprints of a sedimentary fabric can be detected with AMS even for anisotropies as low as 1% (1.01), e.g., Burmeister et al. (2009). In clay-bearing rocks, such overprints result in a reorientation of platy minerals perpendicular to the instantaneous shortening axis (i.e., the LPS) due to tectonic strain. In sandstones, tectonic overprints are typically identified through specific microstructures including transgranular or intra-granular fractures, recrystallization rims, lobate grain boundaries and outcrop-scale structures such as stylolites or deformation bands (e.g., Saint-Bezar et al., 2002).
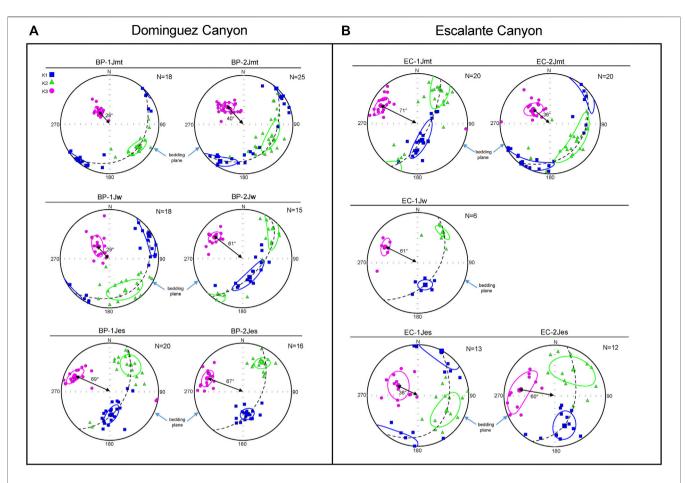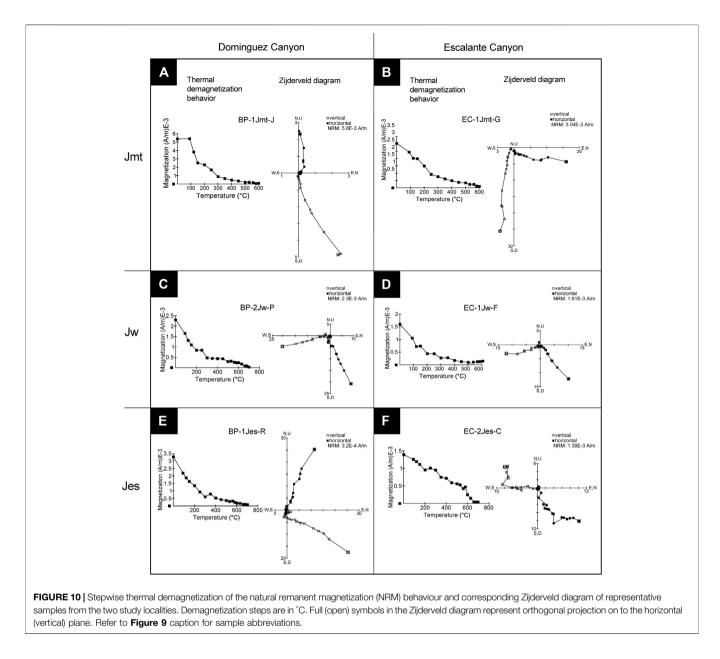
FIGURE 9 | Equal-area lower hemisphere stereographic projections of the three principal magnetic susceptibility axes, including their 95% confidence ellipses around weighted averages derived using Jelinek statistics (1981). Samples in A are from Bridgeport in Dominguez Canyon and B Escalante Canyon (**Figure 1**). Samples are in stratigraphic order from oldest- youngest: Jes, Entrade sandstone; Jw, Wanakah Fm. and Jmt, Tidwell Mbr of the Morrison Fm. K1 in squares, K2 in traingles and K3 in circles. Dotted arc is the K1-K2 plane which defines the magnetic foliation. K1 defines the magnetic lineation. The tilt of magnetic lineation. The tilt of the magnetic fabric, i.e., the deviation of the K3 axis from 90˚ (the sedimentary bedding pole), is represented by the double-headed arrow on the stereonet for each sample.

In the case of the Uncompahgre Uplift rocks investigated in this study, detailed petrographic observations indicate a lack of plastic deformation, beyond rare detrital quartz grain that exhibits pre-existing undulose extinction. The tectonic uplift that occurred in this region resulted in broad-scale tilting of beds, in places up to 10˚. But at our sampling localities, the bedding is close to horizontal (<3 dip). Based on lack of deformation at the scale of the outcrop, the specimen and that of the thin-section, a tectonic origin for the observed AMS fabric can be ruled out. Further, the generally steep attitude (i.e., dip) of the magnetic foliation (~50˚), if it were of tectonic origin, would require an attitude of the shortening axis inconsistent with regional tectonics.

The AMS fabrics of all the specimens are systematically strongly oblique (28–71 dip) with respect to the subhorizontal bedding. Considering this pronounced paradoxical obliquity and the remarkably consistent dip direction to the South East between hand samples from the same site and across the two

sampling sites, a sedimentary origin for the AMS can be ruled out.

To better understand the origin of these magnetic fabrics we need to consider the magnetic minerals present in these rocks. At the outcrop scale, the Entrada Sandstone hand samples commonly show a red color (**Figures 4C**) indicative of the presence of relatively fine hematite. Most specimen also contain relatively large, multi-domain (up to 200 μm) magnetite grains that we interpret as detrital grains based on their rounded and smooth morphology as well as their location in between quartz clasts (**Figure 5**). The hysteresis behavior of most specimens shows a strong contribution from a high magnetic coercivity phase that cannot be magnetite because this mineral typically saturates at the field of 0.2 T or less (e.g., Dunlop and Özdemir, 1997). Hematite and goethite are, in a diagenetic environment, by far the most likely phases responsible for this behavior. The IRM acquisition curves (**Figure 7**) confirm the
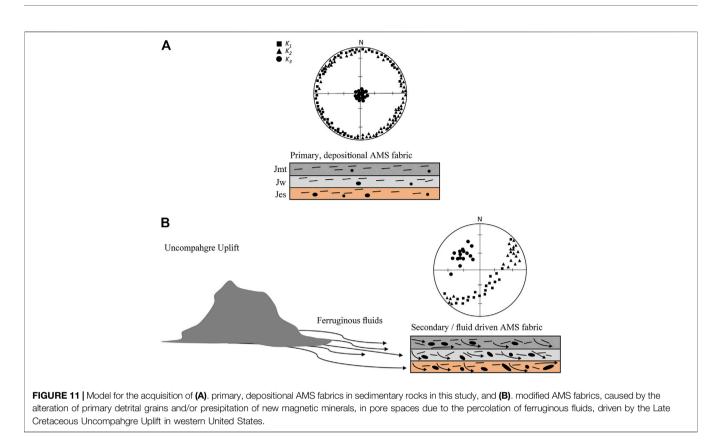
FIGURE 10 | Stepwise thermal demagnetization of the natural remanent magnetization (NRM) behaviour and corresponding Zijderveld diagram of representative samples from the two study localities. Demagnetization steps are in °C. Full (open) symbols in the Zijderveld diagram represent orthogonal projection on to the horizontal (vertical) plane. Refer to **Figure 9** caption for sample abbreviations.

presence of at least one high coercivity phase. Finally, the thermal demagnetization behavior of these rocks shows that in most cases, goethite dominates the NRM, except in the Entrada Formation where hematite contributes more. In general, the magnetic phase carrying the NRM can be—but is not necessarily the same as—the phase carrying the AMS. In summary, most specimens contain a mixture of detrital magnetite (Fe_3O_4), and its typical alteration products; hematite (Fe_2O_3) and goethite $FeO(OH)$. While the absolute percentage of magnetite may be relatively small, this phase contributes substantially to AMS due to its high intrinsic magnetic susceptibility.

While the respective contributions of these three minerals to the AMS of our specimens remain quantitatively unconstrained, their intrinsic magnetic anisotropy may shed light on the origin of

the AMS. Magnetite primarily has a magnetostatic anisotropy (i.e., shape anisotropy) that tends to dominate magnetic fabrics because it has a high magnetic susceptibility (Dunlop and Özdemir, 1997). Hematite, in low fields, has mainly a magnetocrystalline anisotropy that mimics its planar hexagonal shape (Rochette et al., 1992). Goethite grains are elongated along their crystallographic c-axis, which is also the K_3 axis and gives goethite an inverse AMS fabric (e.g., Rochette et al., 1992).

Considering the magnetic assemblage observed in our specimens, two alternative explanations can be proposed:

(1) The competition of goethite, with an inverse AMS fabric fabric (e.g., Martin-Hernandez and García-Hernández, 2010), and hematite + magnetite, with a normal fabric,

FIGURE 11 | Model for the acquisition of **(A)**. primary, depositional AMS fabrics in sedimentary rocks in this study, and **(B)**. modified AMS fabrics, caused by the alteration of primary detrital grains and/or precipitation of new magnetic minerals, in pore spaces due to the percolation of ferruginous fluids, driven by the Late Cretaceous Uncompahgre Uplift in western United States.

may result in inverse or intermediate AMS fabrics depending on the goethite proportion (e.g., Ferré, 2002; Robion et al., 2007).

(2) The percolation of ferruginous fluids through porous sandstones followed by mineral precipitation (**Figure 11B**) may explain the origin of the AMS (e.g., Sizaret et al., 2003; Essalhi et al., 2011).

In these studies, hot fluids precipitate iron oxides and hydroxides in pore spaces of a porous rock and the resulting AMS effectively reflects pore space shape anisotropy.

The first hypothesis cannot explain oblique AMS fabrics because mixtures of normal and inverse AMS fabrics systematically result in perpendicular AMS fabrics (Ferré, 2002). It also seems unlikely because the thermal demagnetization behaviors and magnetic properties of the specimens indicate that the proportion of magnetite, hematite, and goethite varies between hand samples (**Figure 10** and **Tables 1**, **2**).

The second hypothesis is consistent with most observations including the variations in magnetic mineralogy across formation depending on the availability of iron in the environment and possible variations in rock permeability. The fundamental mechanism driving fluids through these formations could be the tectonic uplift of the Uncompahgre mountains which would have caused a regionally consistent hydraulic head to the West of the sampling localities (**Figures 11B**). Although rock fractures are visible at outcrop scale (**Figure 4**), we did not identify any linkage to presence of systematic fracture or pore networks at the microscopic scale (**Figure 5**) and assessing the potential role of fracture networks in contributing to the regional fluid flow through these formation is beyond the scope of this work. Today, the paleomagnetic data showing a reverse period of magnetization at least in the Entrada Formation (e.g., EC-1Jes) supports a Cretaceous precipitation event associated with the Uncompahgre Uplift, although this process is highly unlikely because iron is a very mobile element and subsequent erosion created by the uplift and Quaternary downcutting of the Gunnison River almost certainly created a late-stage fluid flow event to the west.

Magnetic fabrics have previously been used both to characterize fluid flow through porous rocks (e.g., Sizaret et al., 2003; Just et al., 2004; Essalhi et al., 2011) and to quantify pore anisotropy (e.g., Pfleiderer and Halls, 1990; Pfleiderer and Halls, 1993; Benson et al., 2003). Crystallographic analyses of magnetite grains and whether its preferred grain orientation align with pore spaces in the bulk rock (if it exists) are outside the scope of this work. Here in this study of the Uncompahgre Uplift, contrarily to many similar studies of sedimentary rocks using magnetic fabrics, we show that the AMS does not inform on depositional processes, compaction or paleocurrents. Instead, the AMS reflects a regionally consistent post-depositional, tectonically-driven fluid flow owing to cycling via redox reactions of a highly mobile element (Fe) over geologic history in porous and permeable media.

CONCLUSION

The magnetic mineralogy of the Jurassic rocks on the Eastern flank of the Uncompahgre Uplift rocks attests to a primary, detrital magnetite subsequently altered into hematite and goethite. Further dedicated paleomagnetic studies might provide insights into the timing of the uplift and the origin of the oblique foliation symmetry, which we infer might be unrelated to the competition between different phases of ferromagnetic minerals carrying the AMS. This study shows that the AMS fabrics of the Middle-Late Jurassic sandstones of the Uncompahgre Uplift are not primary sedimentary magnetic fabrics. Instead, these fabrics are secondary in origin and most likely developed through unidirectional percolation of Fe-rich fluids that migrated due to the hydraulic head caused by the uplift. Future AMS studies on sedimentary rocks will have to consider that regional hydraulic systems may ultimately affect results and that caution should be exerted in the interpretation of magnetic fabrics.

DATA AVAILABILITY STATEMENT

The original contributions presented in the study are included in the article/**Supplementary Material**, further inquiries can be directed to the corresponding author.

AUTHOR CONTRIBUTIONS

JE did the fieldwork, collected and prepared the samples, performed the AMS, magnetic hysteresis, and IRM experiments, and wrote the first draft of the manuscript. EF advised, provided the lab equipment, directed the research, and edited the successive versions of the manuscript. EF, SS, and JE designed and arranged samples for the thermal demagnetization of the NRM experiment. SS performed the thermal demagnetization of the NRM experiment, took the measurements, and analyzed the data. EF, JE, and SF designed and arranged thin-section samples for SEM. SF performed the SEM experiment, analyzed, and collected the EDS data. JE and EF jointly analyzed all the data. All authors read, edited, and contributed to the final draft of the manuscript.

SUPPLEMENTARY MATERIAL

The Supplementary Material for this article can be found online at: https://www.frontiersin.org/articles/10.3389/feart.2020.601415/full#supplementary-material.

REFERENCES

Aubourg, C., Klootwijk, C., and Korsch, R. J. (2004). Magnetic fabric constraints on oroclinal bending of the Texas and Coffs Harbour blocks: new England Orogen, eastern Australia. *Geol. Soc. Spec. Publ.* 238 (1), 421. doi:10.1144/GSL.SP.2004.238.01.22

Aubourg, C., Smith, B., Eshraghi, A., Lacombe, O., Authemayou, C., Amrouch, K., et al. (2010). New magnetic fabric data and their comparison with palaeostress markers in the Western Fars Arc (Zagros, Iran): tectonic implications. *Geol. Soc. Spec. Publ.* 330 (1), 97. doi:10.1144/SP330.6

Baars, D. and Stevenson, G. (1981). "Tectonic evolution of western Colorado and eastern Utah," in *Western slope (western Colorado) - New Mexico geological society 32nd annual fall field conference guidebook*. Editors R. C. Epis and J. F. Callender (Socorro, NM: New Mexico Geological Society), 337.

Barbeau, D. L. (2003). A flexural model for the Paradox Basin: implications for the tectonics of the ancestral Rocky mountains. *Basin Res.* 15, 97–115. doi:10.1046/j.1365-2117.2003.00194.x

Beitler, B., Parry, W. T., and Chan, M. A. (2005). Fingerprints of Fluid Flow: Chemical Diagenetic History of the Jurassic Navajo Sandstone, Southern Utah, U.S.A, *J. Sediment. Res.* 75, 547–561. doi:10.2110/jsr.2005.045

Benson, P. M., Meredith, P. G., and Platzman, E. S. (2003). Relating pore fabric geometry to acoustic and permeability anisotropy in Crab Orchard Sandstone: A laboratory study using magnetic ferrofluid. *Geophys. Res. Lett.* 30 (19). doi:10.1029/2003gl017929

Burmeister, K. C., Harrison, M. J., Marshak, S., Ferré, E. C., Bannister, R. A., and Kodama, K. P. (2009). Comparison of Fry strain ellipse and AMS ellipsoid trends to tectonic fabric trends in very low-strain sandstone of the Appalachian fold–thrust belt. *J. Struct. Geol.* 31, 1028–1038. doi:10.1016/j.jsg.2009.03.010

Chan, M. A., Ormö, J., Park, A. J., Stich, M., Souza-Egipsy, V., and Komatsu, G. (2007). Models of iron oxide concretion formation: field, numerical, and laboratory comparisons. *Geofluids* 7 (3), 356–368. doi:10.1111/j.1468-8123.2007.00187.x

Chan, M. A., Parry, W. T., and Bowman, J. R. (2000). Diagenetic hematite and manganese oxides and fault-related fluid flow in Jurassic sandstones, Southeastern Utah. *AAPG (Am. Assoc. Pet. Geol.) Bull.* 84, 1281–1310. doi:10.1306/A9673E82-1738-11D7-8645000102C1865D

Cook, K. L., Whipple, K. X., Heimsath, A. M., and Hanks, T. C. (2009). Rapid incision of the Colorado River in Glen Canyon – insights from channel profiles, local incision rates, and modeling of lithologic controls, *Earth Surf. Process. Landforms* 34, 994–1010. doi:10.1002/esp.1790

Dall'Olio, E., Felletti, F., and Muttoni, G. (2013). Magnetic-fabric analysis as a tool to constrain mechanisms of deep-water mudstone deposition in the Marnoso Arenacea Formation (Miocene, Italy). *J. Sediment. Res.* 83, 170–182. doi:10.2110/jsr.2013.12

Davis, G. H. (1978). "Monocline fold pattern of the Colorado Plateau," in *Laramide folding associated with basement block faulting in the western United States*. Editors V. Matthews (Boulder, CO: Geological Society of America), 215–233.

Dunlop, D. J., and Özdemir, Ö. (1997). *Rock magnetism: fundamentals and Frontiers*. Cambridge, UK: Cambridge University Press.

Ejembi, J. I., Potter-McIntyre, S. L., Sharman, G. R., Smith, T. M., Saylor, J. E., Hatfield, K., et al. (in revision). Detrital zircon geochronology and provenance of the Middle to Upper Jurassic Paradox Basin, western Colorado: paleogeographic implications for southwestern Laurentia. *Geosphere*.

Ellwood, B. B., and Howard, J. H. (1981). Magnetic fabric development in an experimentally produced barchan dune, *J. Sediment. Res.* 51, 97–100. doi:10.1306/212F7C16-2B24-11D7-8648000102C1865D

Essalhi, M., Sizaret, S., Barbanson, L., Chen, Y., Branquet, Y., Panis, D., et al. (2009). Track of fluid paleocirculation in dolomite host rock at regional scale by the Anisotropy of Magnetic Susceptibility (AMS): An example from Aptian carbonates of La Florida, Northern Spain. *Earth Planet Sci. Lett.* 277, 501–513. doi:10.1016/j.epsl.2008.11.011

Essalhi, M., Sizaret, S., Barbanson, L., Chen, Y., Lagroix, F., Demory, F., et al. (2011). A case study of the internal structures of gossans and weathering processes in the Iberian Pyrite Belt using magnetic fabrics and paleomagnetic dating. *Miner. Deposita* 46, 981–999. doi:10.1007/s00126-011-0361-8

Ferré, E. C., Bordarier, C., and Marsh, J. S. (2002). Magma flow inferred from AMS fabrics in a layered mafic sill, Insizwa, South Africa. *Tectonophysics* 354, 1–23. doi:10.1016/s0040-1951(02)00273-1

Ferré, E. C. (2002). Theoretical models of intermediate and inverse AMS fabrics. *Geophys. Res. Lett.* 29, 31-1–31-4. doi:10.1029/2001gl014367

Folk, R. L. (1980). *Petrology of sedimentary rocks*. Austin, TX: Hemphill Publishing Company, 182.

Hunt, C. B. (1969). *Geological history of the Colorado river* in *the Colorado river region and John Wesley Powell. U.S. Geological Survey Professional Paper 669-C*. Reston, VA: United States Geological Survey, 59–130.

Hunt, J. M. (1990). Generation and migration of petroleum from abnormally pressured fluid compartments (1). *AAPG (Am. Assoc. Pet. Geol.) Bull.* 74, 1–12.

Ising, G. (1942). On the magnetic properties of varved clay, *Ark. Mat. Astron. Phys.* 29a (5), 1–37.

Jelínek, V. (1978). Statistical processing of anisotropy of magnetic susceptibility measured on groups of specimens. *Studia Geophys. Geod.* 22 (1), 50–62. doi:10.1007/BF01613632

Just, J., Kontny, A., De Wall, H., Hirt, A. M., and Martín-Hernández, F., 2004. Development of magnetic fabrics during hydrothermal alteration in the Soultz-sous-Forets granite from the EPS-1 borehole, Upper Rhine Graben, *Geolo. Soc., London, Special Publications* 238, 509–526. doi:10.1144/gsl.sp.2004.238.01.26

Kelley, V. C. (1958). "Tectonics of the region of the Paradox Basin," in *Guidebook to the Geology of the Paradox Basin: intermountain association of Petroleum Geologists*. Editors A. F. Sanborn (Salt Lake City, UT: Intermountain Association of Petroleum Geologists (U.S.)), 31–38.

Kluth, C. F., and Coney, P. J. (1981). Plate tectonics of the ancestral Rocky Mountains. *Geol.* 9, 10–15. doi:10.1130/0091-7613(1981)9<10:ptotar>2.0.co;2

Lagroix, F., and Banerjee, S. K. (2002). Paleowind directions from the magnetic fabric of loess profiles in central Alaska. *Earth Planet Sci. Lett.* 195, 99–112. doi:10.1016/s0012-821x(01)00564-7

Li, S., Deng, C., Paterson, G. A., Yao, H., Huang, S., Liu, C., et al. (2014). Tectonic and sedimentary evolution of the late Miocene–Pleistocene Dali Basin in the southeast margin of the Tibetan Plateau: Evidences from anisotropy of magnetic susceptibility and rock magnetic data. *Tectonophysics* 629, 362–377. doi:10.1016/j.tecto.2014.05.035

Marshak, S., Karlstrom, K., and Timmons, J. M. (2000). Inversion of Proterozoic extensional faults: An explanation for the pattern of Laramide and Ancestral Rockies intracratonic deformation. *United States, Geolo.* 28, 735–738. doi:10.1130/0091-7613(2000)28<735:iopefa>2.0.co;2

Martin-Hernandez, F., and García-Hernández, M. M. (2010). Magnetic properties and anisotropy constant of goethite single crystals at saturating high fields. *Geophys. J. Int.* 181 (2), 756–761. doi:10.1111/j.1365-246X.2010.04566.x

Massei, N., Lacroix, M., Wang, H. Q., and Dupont, J.-P. (2002). Transport of particulate material and dissolved tracer in a highly permeable porous medium: comparison of the transfer parameters. *J. Contam. Hydrol.* 57, 21–39. doi:10.1016/s0169-7722(01)00216-9

McFadden, P. L., and McElhinny, M. W. (1990). Classification of the reversal test in palaeomagnetism. *Geophys. J. Int.* 103, 725–729. doi:10.1111/j.1365-246x.1990.tb05683.x

Musgrove, M., and Banner, J. L. (1993). Regional ground-water mixing and the origin of saline fluids: midcontinent, United States. *Science* 259, 1877–1882. doi:10.1126/science.259.5103.1877

Nuccio, V. F., and Condon, S. M. (1996). *Burial and thermal history of the Paradox Basin, Utah and Colorado, and petroleum potential of the Middle Pennsylvanian Paradox Basin, U.S. Geol. Survey Bulletin 2000-O*. Boston, MA: U.S. Government Printing Office, 57–76.

Oliver, J. (1986). Fluids expelled tectonically from orogenic belts: Their role in hydrocarbon migration and other geologic phenomena. *Geol.* 14, 99–102. doi:10.1130/0091-7613(1986)14<99:fetfob>2.0.co;2

Parés, J. M., Hassold, N. J. C., Rea, D. K., and van der Pluijm, B. A. (2007). Paleocurrent directions from paleomagnetic reorientation of magnetic fabrics in deep-sea sediments at the Antarctic Peninsula Pacific margin (ODP Sites 1095, 1101). *Mar. Geol.* 242, 261–269. doi:10.1016/j.margeo.2007.04.002

Parés, J. M., Miguens, L., and Saiz, C. (2016). Characterizing pore fabric in sandstones with magnetic anisotropy methods: Initial results. *J. Petrol. Sci. Eng.* 143, 113–120. doi:10.1016/j.petrol.2016.02.028

Parry, W. T., Chan, M. A., and Beitler, B. (2004). Chemical bleaching indicates episodes of fluid flow in deformation bands in sandstone. *AAPG Bulletin* 88, 175–191. doi:10.1306/09090303034

Pederson, J. L., Mackley, R. D., and Eddleman, J. L. (2002). Colorado Plateau uplift and erosion evaluated using GIS. *GSA Today (Geol. Soc. Am.)* 12, 4–10. doi:10.1130/1052-5173(2002)012<0004:cpuaee>2.0.co;2

Pfleiderer, S., and Halls, H. C. (1993). Magnetic pore fabric analysis: Verification through image autocorrelation. *J. Geophys. Res.* 98, 4311–4316. doi:10.1029/92jb01851

Pfleiderer, S., and Halls, H. C. (1990). Magnetic susceptibility anisotropy of rocks saturated with ferrofluid: a new method to study pore fabric? *Phys. Earth Planet. In.* 65, 158–164. doi:10.1016/0031-9201(90)90083-a

Potter, S. L., and Chan, M. A. (2011). Joint controlled fluid flow patterns and iron mass transfer in Jurassic Navajo Sandstone. *Geofluids* 11, 184–198. doi:10.1111/j.1468-8123.2011.00329.x

Potter-McIntyre, S. L., Chan, M. A., and McPherson, B. J. (2014). Concretion formation in volcaniclastic host rocks: evaluating the role of organics, mineralogy, and geochemistry on early diagenesis. *J. Sediment. Res.* 84, 875–892. doi:10.2110/jsr.2014.58

Rønnevik, C., Ksienzyk, A. K., Fossen, H., and Jacobs, J. (2017). Thermal evolution and exhumation history of the Uncompahgre Plateau (northeastern Colorado Plateau), based on apatite fission track and (U-Th)-He thermochronology and zircon U-Pb dating *Geosphere* 13, 518–537. doi:10.1130/GES01415.1.

Robion, P., David, C., Dautriat, J., Colombier, J.-C., Zinsmeister, L., and Collin, P.-Y. (2014). Pore fabric geometry inferred from magnetic and acoustic anisotropies in rocks with various mineralogy, permeability and porosity. *Tectonophysics* 629, 109–122. doi:10.1016/j.tecto.2014.03.029

Robion, P., Grelaud, S., and Frizon de Lamotte, D. (2007). Pre-folding magnetic fabrics in fold-and-thrust belts: Why the apparent internal deformation of the sedimentary rocks from the Minervois basin (NE-Pyrenees, France) is so high compared to the Potwar basin (SW-Himalaya, Pakistan)? *Sediment. Geol.* 196, 181–200. doi:10.1016/j.sedgeo.2006.08.007

Rochette, P., Jackson, M., and Aubourg, C. (1992). Rock magnetism and the interpretation of anisotropy of magnetic susceptibility. *Rev. Geophys.* 30, 209–226. doi:10.1029/92rg00733

Saint-Bezar, B., Hebert, R. L., Aubourg, C., Robion, P., Swennen, R., and de Lamotte, D. F. (2002). Magnetic fabric and petrographic investigation of hematite-bearing sandstones within ramp-related folds: examples from the South Atlas Front (Morocco). *J. Struct. Geol.* 24, 1507–1520. doi:10.1016/s0191-8141(01)00140-7

Schieber, J. and Ellwood, B. B. (1993). Determination of basinwide paleocurrent patterns in a shale succession from anisotropy of magnetic susceptibility (AMS); a case study of the mid-Proterozoic Newland Formation, Montana. *J. Sediment. Res.* 63, 874–880.

Sizaret, S., Chen, Y., Barbanson, L., Henry, B., Camps, P., and Marcoux, E. (2006). Crystallization in flow–I. Palaeocirculation track by texture analysis and magnetic fabrics. *Geophys. J. Int.* 167, 605–612. doi:10.1111/j.1365-246x.2006.03106.x

Sizaret, S., Chen, Y., Chauvet, A., Marcoux, E., and Touray, J. C. (2003). Magnetic fabrics and fluid flow directions in hydrothermal systems. A case study in the Chaillac Ba–F–Fe deposits (France). *Earth Planet Sci. Lett.* 206, 555–570. doi:10.1016/s0012-821x(02)01112-3

Tarling, D. H., and Hrouda, F. (1993). *The Magnetic anisotropy of rocks*. Berlin, Germany: Springer, 218.

Tweto, O., and Schoenfeld, R. (1979). *Geologic map of Colorado*. Reston, VA: U.S. Geological Survey.

Ungerer, P., Burrus, J., Doligez, B., Chenet, P., and Bessis, F. (1990). Basin evaluation by integrated two-dimensional modeling of heat transfer, fluid flow, hydrocarbon generation, and migration (1). *AAPG (Am. Assoc. Pet. Geol.) Bull.* 74, 309–335.

Wilkinson, J. J. (2001). Fluid inclusions in hydrothermal ore deposits. *Lithos* 55, 229–272. doi:10.1016/s0024-4937(00)00047-5

Wing, B. A., and Ferry, J. M. (2007). Magnitude and geometry of reactive fluid flow from direct inversion of spatial patterns of geochemical alteration. *Am. J. Sci.* 307, 793–832. doi:10.2475/05.2007.02